Supplementary Material

Extraordinary altruists exhibit enhanced self-other overlap in neural responses to distress

Kristin M. Brethel-Haurwitz[1*], Elise M. Cardinale[2], Kruti M. Vekaria[2], Emily L. Robertson[3], Brian Walitt[4], John W. VanMeter[5], & Abigail A. Marsh[2]

[1]Department of Psychology, University of Pennsylvania, Philadelphia, PA 19104.

[2]Department of Psychology, Georgetown University, Washington DC 20057.

[3]Department of Psychology, Louisiana State University, Baton Rouge LA 70803.

[4]National Institute of Nursing Research, National Institutes of Health, Bethesda MD 20892.

[5]Department of Neurology, Georgetown University Medical Center, Washington DC 20057.

*Correspondence to: kbreth@sas.upenn.edu.

Supplementary Material includes:

Supplementary Methods

Neuroimaging Acquisition

MR images were acquired with a 3T Siemens Tim Trio scanner (Siemens Medical Solutions) and a 12-channel phased-array head coil. Functional data were collected using a T2*-weighted echo-planar imaging sequence (46 3.0 mm transversal slices; 64 × 64 matrix; repetition time, 2,500 ms; echo time, 30 ms; field of view, 192 mm^2; 3.0 × 3.0 × 3.0 mm voxels). The first four volumes of each functional run were excluded from analysis to account for magnet stabilization. High-resolution T1-weighted anatomical images were also acquired (3D Magnetization Prepared Rapid Acquisition Gradient Echo; 176 1.0-mm axial slices; field of view, 250 mm^2; repetition time, 1,900 ms; echo time, 2.52 ms; 246 × 256 matrix).

Analysis of Neuroimaging Data

Functional data were preprocessed and analyzed according to the general linear model, using Analysis of Functional NeuroImages (AFNI) (Cox, 1996). The three runs of the task were concatenated, despiked, motion-corrected, and spatially smoothed using a 6 mm full-width half maximum Gaussian filter. TRs with greater than 0.5 mm frame displacement were censored during preprocessing. Functional data were aligned to the anatomical grid, linearly transformed to a Talairach space template (the detailed TT_N27 template created from 27 scans of one individual), and masked with an extents mask to account for motion artifacts and to exclude voxels without valid data at every TR for every run, helping to control for false activations. Twelve regressors were created to model the anticipation and stimulation portions of each run, resulting in the following four regressors for each run: threat (cue indicates potential pain), no threat (safety cue), pain (stimulation), no pain (no stimulation). For each participant, contrasts

were also calculated for pain (pain > no pain) and threat (threat > no threat) for each run. Rest was modeled implicitly; baseline was modeled by a first-order function, and motion artifacts were modeled using the six estimated rigid-body motion parameters. Boxcar regressors representing the occurrence of each block type were convolved with a canonical hemodynamic response function, scaled to an amplitude of 1.

Group-level analyses were limited to a brain mask defined by voxels with functional activation shared by at least 50% of participants. Cluster size thresholds were calculated for a corrected clusterwise p threshold of .05, at uncorrected $p = .001$, for this group mask for each comparison using 10,000 Monte Carlo simulations conducted in conjunction with 3dttest++ (via the -Clustsim option) in AFNI (October 2016 AFNI version 16.3.03, using a nonparametric randomization approach to generate cluster size thresholds from the residuals of each t test to decrease risk of false positives (Cox, Chen, Glen, Reynolds, & Taylor, 2017), created in response to Eklund et al. (Eklund, Nichols, & Knutsson, 2016)). MNI coordinates of peak z statistics within significant clusters are reported. Region labels are reported according to the CA N27 ML atlas (Eickhoff et al., 2005) in AFNI. As noted above, final administered pressure stimulation level was included as a centered covariate in analyses of experienced pain and threat given the significant group difference, to examine group differences due to subjective experience rather than objective pressure stimulation level. The covariate was mean centered across all participants, so as to not artificially remove group differences in this variable.

In order to examine group differences in similarity of neural activation for experienced and empathic pain and threat, conservative conjunction-null analyses (Nichols, Brett, Andersson, Wager, & Poline, 2005) were conducted in which activation maps meeting statistical thresholds in each condition were compared, such that regions of conjunction indicated significant

activation in both conditions independently, an approach that has been utilized in examining similarity between *self* and *other* responses in empathic pain paradigms (e.g., Beckes et al., 2012). Specifically, a mask was created from a thresholded *self pain* > *self no pain* contrast with objective pain level as a covariate of no interest, and this mask was then applied to an *other pain* > *other no pain* contrast, as paired samples *t* tests within each group. Parallel contrasts were conducted for the threat conditions. Analyses were also conducted in which self-reported connectedness with the study partner and immediate family were separately included as covariates of no interest, centered across all participants, in contrasts at the *other* level. Following up on conjunction patterns observed at the group level, covariation analyses were conducted, in which the association between *self* and *other* activation levels in regions of interest were tested via partial correlation controlling for objective pain level, to determine if apparent self-other mapping at the group level in conjunction analyses were supported by individual-level correspondence in neural activation. Regions of interest (ROIs) in bilateral anterior insula (AI) were defined by 5 mm radius spheres centered at coordinates (left AI: x = -40, y = 22, z = 0; right AI: x = 39, y = 23, z = -4) derived from a functional meta-analysis of empathic pain studies (Lamm et al., 2011).

Generalized psychophysiological interaction (gPPI) functional connectivity analyses were conducted in SPM8 (Wellcome Trust Department of Cognitive Neurology) using the generalized PPI toolbox (McLaren, Ries, Xu, & Johnson, 2012). Functional images were slice-time corrected, realigned, coregistered to anatomical scans, normalized to 2.0 × 2.0 × 2.0 mm voxel size in MNI space using parameters calculated during segmentation of anatomical scans, and smoothed using a 6 mm Gaussian kernel. Task-specific functional connectivity with left AI was estimated using gPPI analysis (McLaren et al., 2012). The AI seed region was the same ROI

sphere used above. The *other* and *self* runs were processed separately, such that functional connectivity in one run was not controlling for the other. A design matrix was created for each participant that included the stimulus time series for each of the four conditions (threat, no threat, pain, no pain) and six motion parameters, which were convolved with a hemodynamic response function to create psychological regressors. Within each condition, examining connectivity during threat experience was holding the other three conditions (no threat, pain, no pain) constant, and was thus specific to threat. Analogous contrasts were conducted for pain experience. Functional connectivity specific to the threat and pain conditions within the *other* run are the focus of the analyses reported here. Functional connectivity results were limited to a set of bilateral *a priori* ROIs for the two conditions (threat: amygdala, hypothalamus, periaqueductal gray, ventromedial prefrontal cortex, insula; pain: anterior cingulate cortex, periaqueductal gray, inferior parietal cortex, insula). All regions were defined using the AAL atlas (Tzourio-Mazoyer et al., 2002), except for the periaqueductal gray and hypothalamus. The periaqueductal gray was defined as two 5 mm radius spheres centered at the average coordinates for left and right activation ($x = \pm 4$, $y = -29$, $z = -12$) from a recent meta-analysis (Linnman, Moulton, Barmettler, Becerra, & Borsook, 2012). The hypothalamus ROI was defined using the Talairach Daemon label (Lancaster et al., 2000) in the WFU PickAtlas Tool (Maldjian, Laurienti, Kraft, & Burdette, 2003). The PickAtlas Tool was used to create all ROI masks. Nonparametric clusterwise inference was computed via the SnPM13 toolbox (http://warwick.ac.uk/snpm) in SPM8, at an FWE corrected threshold of $p = .05$ at an uncorrected $p = .001$, using 10,000 permutations. Reported results are from the output of these SnPM simulations. Independent samples *t* tests (altruists > controls) were conducted separately on the threat and pain contrasts to directly

compare group differences in functional connectivity of the left AI during empathic threat and pain. MNI coordinates of peak *t* statistics within significant clusters are reported.

Two sets of follow-up control analyses were conducted in order to examine the robustness of our neural results: (1) repetition of analyses excluding 6 altruistic kidney donors who directed their donation to a specific stranger, (2) repetition of analyses in the full sample with the addition of household income and education as binary covariates of no interest, given trends toward group differences in these demographic variables (see Table 1). In the second set of analyses, covariates were mean centered across all participants and included at both the self and other levels of conjunction analyses. In the second set of control analyses, one control was excluded since income was not reported.

Supplementary References

Cox, R. W. (1996). AFNI: Software for analysis and visualization of functional magnetic resonance neuroimages. *Computers and Biomedical Research, 29*(3), 162-173.

Cox, R. W., Chen, G., Glen, D. R., Reynolds, R. C., & Taylor, P. A. (2017). FMRI clustering in AFNI: False positive rates redux. *Brain Connectivity, 7*(3), 152-171.

Eickhoff, S. B., Stephan, K. E., Mohlberg, H., Grefkes, C., Fink, G. R., Amunts, K., & Zilles, K. (2005). A new SPM toolbox for combining probabilistic cytoarchitectonic maps and functional imaging data. *Neuroimage, 25*(4), 1325-1335. doi:10.1016/j.neuroimage.2004.12.034

Eklund, A., Nichols, T. E., & Knutsson, H. (2016). Cluster failure: Why fMRI inferences for spatial extent have inflated false-positive rates. *Proceedings of the National Academy of Sciences, 113*(28), 7900-7905. doi: 10.1073/pnas.1602413113

Lancaster, J. L., Woldorff, M. G., Parsons, L. M., Liotti, M., Freitas, C. S., Rainey, L., . . . Fox, P. T. (2000). Automated Talairach atlas labels for functional brain mapping. *Human Brain Mapping, 10*(3), 120-131. doi:10.1002/1097-0193(200007)10:3%3C120::AID-HBM30%3E3.0.CO;2-8

Linnman, C., Moulton, E. A., Barmettler, G., Becerra, L., & Borsook, D. (2012). Neuroimaging of the periaqueductal gray: State of the field. *Neuroimage, 60*(1), 505-522. doi:10.1016/j.neuroimage.2011.11.095

Maldjian, J. A., Laurienti, P. J., Kraft, R. A., & Burdette, J. H. (2003). An automated method for neuroanatomic and cytoarchitectonic atlas-based interrogation of fMRI data sets. *NeuroImage, 19*(3), 1233-1239. doi:10.1016/S1053-8119(03)00169-1

McLaren, D. G., Ries, M. L., Xu, G., & Johnson, S. C. (2012). A generalized form of context-

dependent psychophysiological interactions (gPPI): A comparison to standard approaches. *Neuroimage, 61*(4), 1277-1286. doi:10.1016/j.neuroimage.2012.03.068

Nichols, T., Brett, M., Andersson, J., Wager, T., & Poline, J. B. (2005). Valid conjunction inference with the minimum statistic. *Neuroimage*, *25*(3), 653-660. doi:10.1016/j.neuroimage.2004.12.005

Tzourio-Mazoyer, N., Landeau, B., Papathanassiou, D., Crivello, F., Etard, O., Delcroix, N., . . . Joliot, M. (2002). Automated anatomical labeling of activations in SPM using a macroscopic anatomical parcellation of the MNI MRI single-subject brain. *Neuroimage*, *15*(1), 273-289. doi:10.1006/nimg.2001.0978

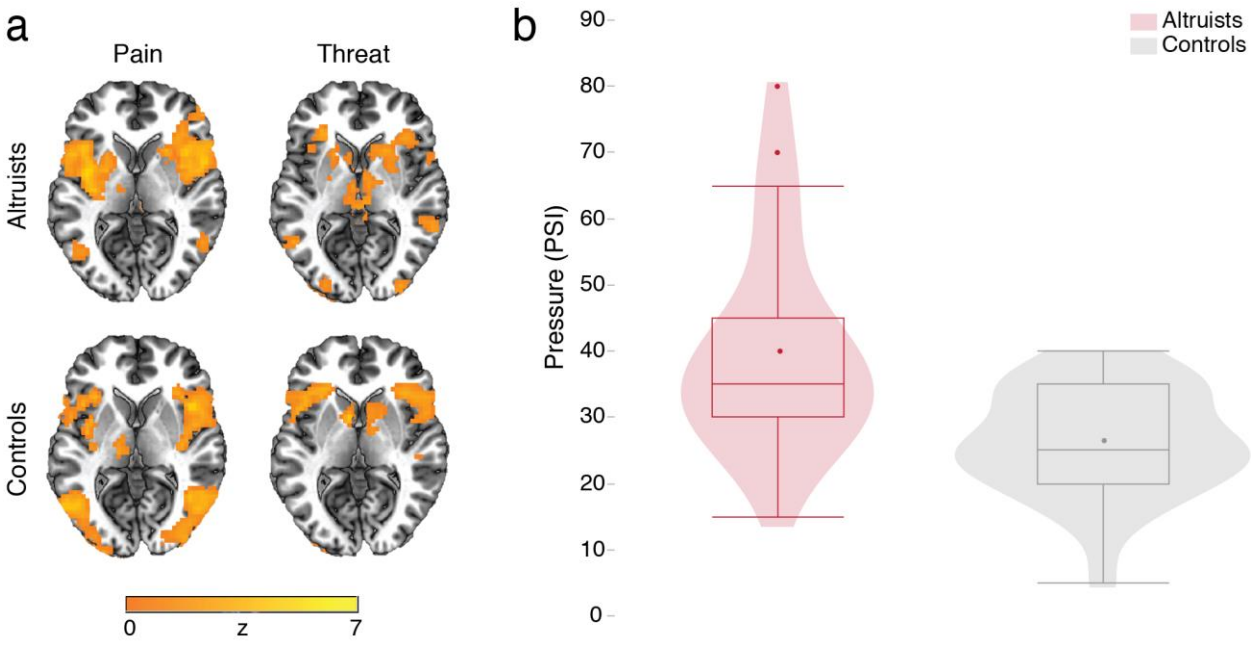

Figure S1. Self pain and threat results and pressure stimulation levels. (a) Altruists and controls exhibited similar neural activation for *self pain* > *self no pain* and *self threat* > *self no threat*. z = 0. Whole-brain clusterwise corrected threshold $p < .05$ at uncorrected voxelwise threshold $p = .001$ (b) Final subjective "slightly intense" pain level selected by each group. Altruists selected a significantly higher pressure level than controls, $t(50) = 3.97$, $p < .001$, $d = 1.10$ [95% CI: 0.51-1.68]. Contours represent frequency distributions. Boxplots are displayed with dots representing means and outliers.

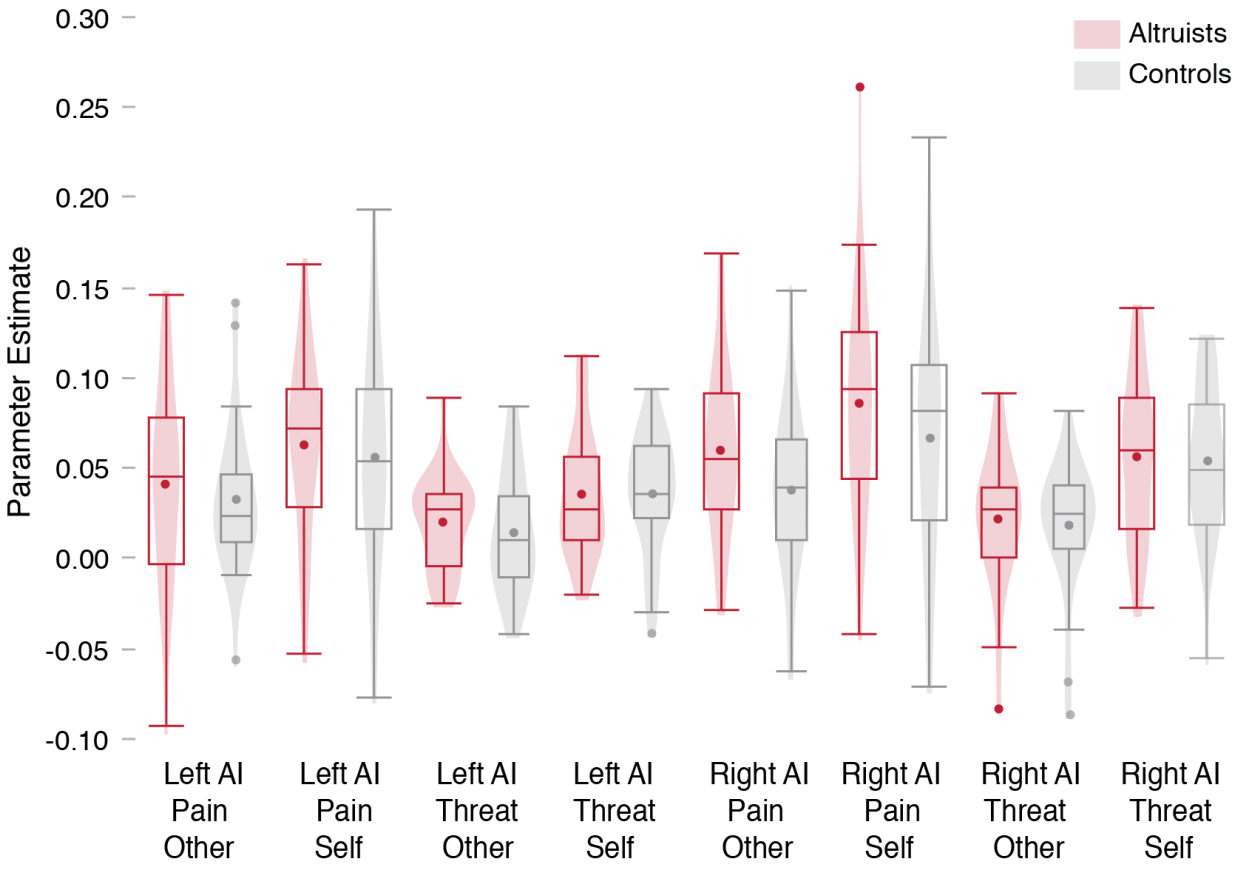

Figure S2. Parameter estimates for mean activation in left and right anterior insula (AI) ROIs. Contours represent frequency distributions. Boxplots are displayed with dots representing means and outliers. Parameter estimates for pain and threat are relative to condition-specific baselines (pain > no pain, threat > no threat). There were no group differences in activation for any AI ROI, all $p > .05$, all $d < 0.48$. Across all participants, *self* pain resulted in higher activation than *other* pain in left AI, $t(51) = 2.39$, $p = .020$, $d = 0.41$, and right AI, $t(51) = 2.79$, $p = .007$, $d = 0.47$, and *self* threat resulted in higher activation than *other* threat in left AI, $t(51) = 3.11$, $p = .003$, $d = 0.59$, and right AI, $t(51) = 4.92$, $p < .001$, $d = 0.87$. However, pain activation was higher than threat activation for the *self* in left AI, $t(51) = 3.39$, $p = .001$, $d = 0.49$, and right AI, $t(51) = 2.20$, $p = .033$, $d = 0.37$, and pain activation was also higher than threat activation for *other* in left AI, $t(51) = 2.41$, $p = .020$, $d = 0.49$, and right AI, $t(51) = 3.71$, $p = .001$, $d = 0.69$.

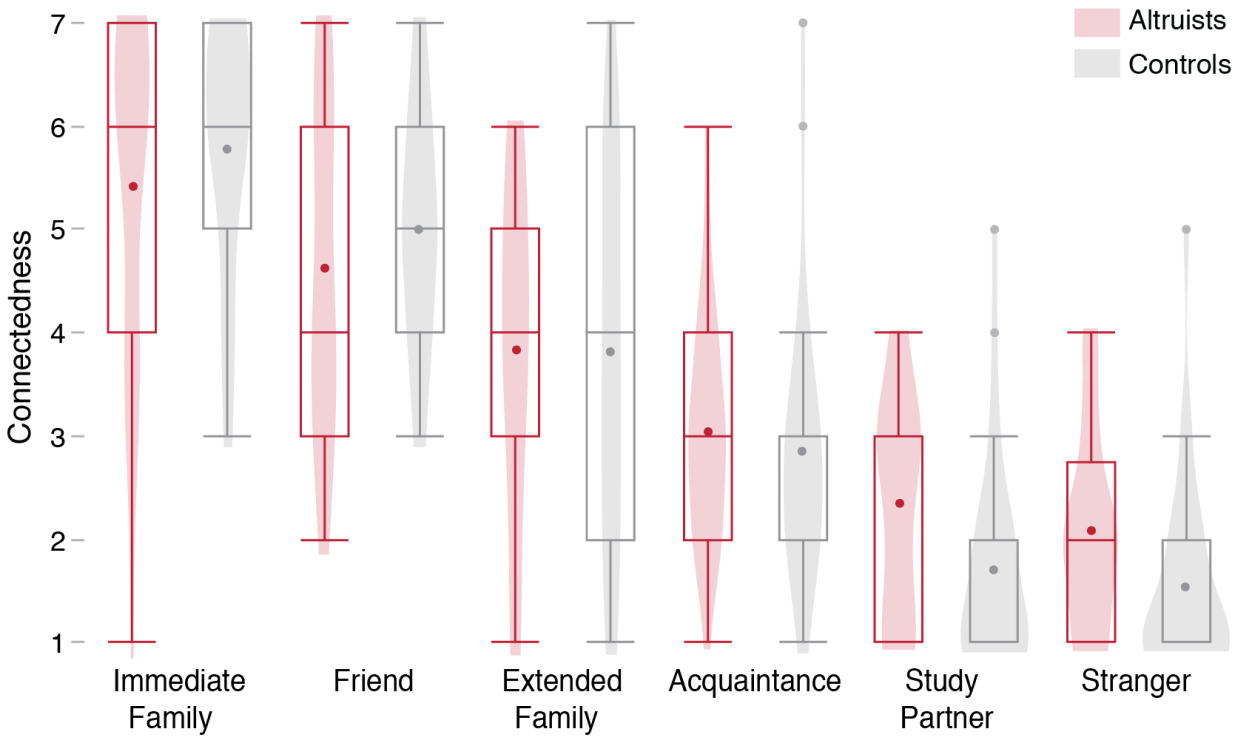

Figure S3. Perceptions of connectedness as rated on the Inclusion of Other in the Self Scale. Contours represent frequency distributions. Boxplots are displayed with dots representing means and outliers. Altruists rated greater connectedness for the study partner and strangers in general, both $p \leq .05$, both $d > 0.56$.

Table S1

Correlations between Connectedness, Self-Reported Empathy, and Activation in Bilateral Anterior Insula ROIs in Each Group

		IoS Study Partner	IRI Empathic Concern	EPS Empathic Concern	L AI Pain Self	R AI Pain Self	L AI Fear Self	R AI Fear Self	L AI Pain Other	R AI Pain Other	L AI Fear Other	R AI Fear Other
Altruists	IoS Stranger[a]	.70**†[b]	.60**†	.58**†	-.18	-.20	-.23	.04	-.38	-.44*	.29	.28
	IoS Study Partner[b]		.23	.52*	.05	-.33	-.38	-.13	-.32	-.33	-.01	.32
	IRI Empathic Concern			.52**	.01	-.12	-.12	.01	-.16	-.20	.41*	.47*
	EPS Empathic Concern				-.25	-.35	-.37	-.19	-.23	-.36	.13	.31
	L AI Pain Self					.49*	.39	.24	.57**†	.52**	-.23	.06
	R AI Pain Self						.27	.22	.38	.29	-.33	-.50*
	L AI Fear Self							.79**†	.26	.46*	.28	-.12
	R AI Fear Self								.13	.40*	.21	-.02
	L AI Pain Other									.74**†	-.19	.10
	R AI Pain Other										-.12	.14
	L AI Fear Other											.56**†
Controls	IoS Stranger[c]	.78**†	.18	.40*	.32	.22	.38	.38	-.02	.08	.30	.30
	IoS Study Partner		.34	.44*	.25	.26	.27	.31	-.13	.05	.37	.43*
	IRI Empathic Concern			.61**†	-.15	.10	-.19	.02	.26	.50**	.20	.12
	EPS Empathic Concern				-.03	.07	-.10	-.08	.33	.36	.09	.13
	L AI Pain Self					.42*	.56**†	.22	-.23	-.10	.04	.20
	R AI Pain Self						.11	.38*	.15	.21	.19	.31
	L AI Fear Self							.55**†	-.29	-.11	-.02	.33
	R AI Fear Self								.07	.12	.28	.39*
	L AI Pain Other									.80**†	.05	.01
	R AI Pain Other										.14	.16
	L AI Fear Other											.58**†

Note. Altruist N = 25, Control N = 27, unless otherwise noted. ROI = region of interest. IoS = Inclusion of Other in Self. IRI = Interpersonal Reactivity Index. EPS = Empathy for Pain Scale. L = left. R = right. AI = anterior insula.
[a]N = 24. [b]N = 23. [c]N = 26.
*p < .05. **p < .01. †Q < .05 per Benjamini-Hochberg procedure for 66 tests within each group.

Table S2

Regions of Significant Activation for Other Pain > Other No Pain, Masked by Self Pain > Self No Pain, in Each Group

Altruists					
k[a]	Peak x	Peak y	Peak z	Peak *z*(24)	Peak Region
319	56	21	3	6.09	Right Inferior Frontal Gyrus
290	-62	-30	45	6.05	Left Inferior Parietal Lobule
286	66	-38	24	6.42	Right Supramarginal Gyrus
234	-49	-74	-4	6.76	Left Inferior Occipital Gyrus
150	50	-59	-5	6.20	Right Inferior Temporal Gyrus
46	-46	13	17	4.59	Left Inferior Frontal Gyrus
43	47	9	56	5.78	Right Middle Frontal Gyrus
42	-40	17	0	4.65	Left Insula
33	50	48	5	4.44	Right Middle Frontal Gyrus
28	-24	-65	-48	4.18	Left Cerebellum
27	31	-46	42	4.97	Right Inferior Parietal Lobule
21	-30	-16	-1	4.70	Left Putamen
17	8	9	52	4.94	Right Supplementary Motor Area
15	-11	-8	9	4.11	Left Thalamus
11	12	-8	12	3.82	Right Thalamus
10	-8	-24	37	4.03	Left Middle Cingulate Cortex
9	-24	1	-13	4.52	Left Putamen
Controls					
k[b]	Peak x	Peak y	Peak z	Peak *z*(26)	Peak Region
961	53	-68	-1	7.03	Right Middle Temporal Gyrus
715	-56	-24	41	6.33	Left Inferior Parietal Lobule
710	-46	-71	-1	6.77	Left Middle Occipital Gyrus
615	56	-21	37	6.37	Right Postcentral Gyrus
238	53	11	35	5.95	Right Precentral Gyrus
134	-4	-80	-41	4.77	Left Cerebellum
29	-53	10	28	5.44	Left Inferior Frontal Gyrus
26	43	2	-3	4.51	Right Insula
19	24	-54	63	4.45	Right Superior Parietal Lobule
15	12	-74	-44	5.63	Right Cerebellum

[a]Cluster extent for clusterwise corrected threshold $p < .05$ at uncorrected $p = .001 = 8$ voxels
[b]Cluster extent for clusterwise corrected threshold $p < .05$ at uncorrected $p = .001 = 10$ voxels

Table S3

Regions of Significant Activation for Other Threat > Other No Threat, Masked by Self Threat > Self No Threat, in Each Group

Altruists					
k[a]	Peak x	Peak y	Peak z	Peak *z*(24)	Peak Region
28	-30	23	-11	4.47	Left Inferior Frontal Gyrus
20	2	24	55	4.84	Left Supplementary Motor Area
19	-56	-47	25	4.72	Left Supramarginal Gyrus
18	34	-96	4	4.02	Right Middle Occipital Gyrus
16	31	26	-4	3.96	Right Insula
15	-20	-96	-3	3.73	Left Middle Occipital Gyrus
5	2	44	36	4.15	Left Superior Medial Gyrus
Controls					
k[b]	Peak x	Peak y	Peak z	Peak *z*(26)	Peak Region
16	50	24	3	4.31	Right Inferior Frontal Gyrus
14	-33	-96	1	3.92	Left Middle Occipital Gyrus
12	31	32	-5	3.64	Right Inferior Frontal Gyrus
10	-59	-21	30	3.92	Left Postcentral Gyrus
7	8	9	11	3.99	Right Caudate Nucleus
7	59	-47	25	3.90	Right Supramarginal Gyrus
4	-27	-87	-7	3.56	Left Inferior Occipital Gyrus
4	-33	-40	42	3.57	Left Inferior Parietal Lobule
4	-43	-45	56	4.05	Left Inferior Parietal Lobule

[a]Cluster extent for clusterwise corrected threshold $p < .05$ at uncorrected $p = .001 = 5$ voxels
[b]Cluster extent for clusterwise corrected threshold $p < .05$ at uncorrected $p = .001 = 4$ voxels

Table S4

Regions of Significant Activation for Self Pain > Self No Pain in Each Group

Altruists					
k[a]	Peak x	Peak y	Peak z	Peak *z*(23)	Peak Region
1557	-40	-2	-2	5.97	Left Insula
940	37	6	4	5.77	Right Insula
469	62	-34	34	5.88	Right Supramarginal Gyrus
351	28	-51	-26	5.34	Right Cerebellum
334	-1	8	42	5.64	Left Middle Cingulate Cortex
285	-30	-63	-25	5.22	Left Cerebellum
179	-4	25	-14	-4.33	Left Middle Orbital Gyrus
59	8	-32	65	-4.12	Right Paracentral Lobule
45	8	-13	-5	5.00	Right Thalamus
40	-14	-27	37	4.58	Left Middle Cingulate Cortex
36	-20	-71	-51	4.85	Left Cerebellum
32	34	-40	42	4.13	Right Supramarginal Gyrus
Controls					
k[b]	Peak x	Peak y	Peak z	Peak *z*(25)	Peak Region
1644	-53	-24	41	6.34	Left Inferior Parietal Lobule
1303	-59	-64	9	5.44	Left Middle Temporal Gyrus
1157	28	-88	-10	5.34	Right Inferior Occipital Gyrus
946	56	-26	20	6.30	Right Rolandic Operculum
736	53	15	10	6.08	Right Inferior Frontal Gyrus
376	5	8	35	5.16	Right Middle Cingulate Cortex
264	-56	20	-11	5.74	Left Temporal Pole
37	8	-32	69	-4.57	Right Paracentral Lobule
35	-33	43	15	4.11	Left Middle Frontal Gyrus

[a]Cluster extent for clusterwise corrected threshold $p < .05$ at uncorrected $p = .001$ =27 voxels
[b]Cluster extent for clusterwise corrected threshold $p < .05$ at uncorrected $p = .001$ = 30 voxels

Table S5

Regions of Significant Activation for Self Threat > Self No Threat in Each Group

Altruists					
k[a]	Peak x	Peak y	Peak z	Peak *z*(23)	Peak Region
836	18	12	11	5.25	Right Caudate Nucleus
359	-1	33	51	5.45	Left Superior Medial Gyrus
278	43	2	49	4.54	Right Precentral Gyrus
202	-30	-90	-3	4.71	Left Middle Occipital Gyrus
188	-56	-47	32	4.70	Left Supramarginal Gyrus
155	66	-44	28	4.73	Right Supramarginal Gyrus
126	28	-93	-3	5.41	Right Inferior Occipital Gyrus
101	-1	-54	-32	4.23	Cerebellar Vermis
74	-27	29	-4	4.81	Left Insula
47	-53	-58	8	4.55	Left Middle Temporal Gyrus
46	59	-46	1	4.42	Right Middle Temporal Gyrus
45	43	-64	-28	4.28	Right Cerebellum
Controls					
k[b]	Peak x	Peak y	Peak z	Peak *z*(25)	Peak Region
323	47	23	-11	5.44	Right Inferior Frontal Gyrus
290	-30	26	-8	5.07	Left Insula
260	-59	-21	37	4.97	Left Supramarginal Gyrus
220	2	18	55	4.63	Right Supplementary Motor Area
143	12	9	11	5.44	Right Caudate Nucleus
142	-24	-94	-6	4.62	Left Inferior Occipital Gyrus
131	53	-25	24	5.56	Right Rolandic Operculum
99	-8	8	0	5.52	Left Caudate Nucleus
59	43	5	46	4.67	Right Precentral Gyrus
52	-46	5	46	4.31	Left Precentral Gyrus
32	53	-27	-7	4.62	Right Middle Temporal Gyrus

[a]Cluster extent for clusterwise corrected threshold $p < .05$ at uncorrected $p = .001 = 43$ voxels
[b]Cluster extent for clusterwise corrected threshold $p < .05$ at uncorrected $p = .001 = 29$ voxels

Table S6

Significant Functional Connectivity with Left AI for Altruists > Controls for Other Pain and Other Threat

Other Pain					
k[a]	Peak x	Peak y	Peak z	Peak *t*(50)	ROI
18[b]	-38	14	0	3.88	Left Insula
11[b]	-44	4	8	3.87	Left Insula
Other Threat					
k[a]	Peak x	Peak y	Peak z	Peak *t*(50)	ROI
14[b]	-32	20	-12	4.08	Left Insula
9[c]	-24	-2	-16	2.98	Left Amygdala

[a]$2mm^3$ voxels
[b]Cluster extent for clusterwise corrected threshold $p < .05$ at uncorrected $p = .001 = 8$ voxels
[c]Cluster extent for clusterwise corrected threshold $p < .05$ at uncorrected $p = .005 = 3$ voxels